

Complex resistivity tomography for environmental applications

Andreas Kemna^{a,*}, Andrew Binley^b, Abelardo Ramirez^c, William Daily^c

^a DMT-GeoTec Division, Essen D-45307, Germany

^b Lancaster University, Lancaster, LA1 4YQ, UK

^c Lawrence Livermore National Laboratory, Livermore, CA 94550, USA

Abstract

Complex resistivity may provide valuable information about the structural and hydraulic nature of porous media and fluids contained within such media. The environmental value of such a property is obvious. To date most environmental applications of complex resistivity have focussed on relatively crude data analysis methods and restrictive electrode configurations. New tomographic methods are becoming available that will allow complex resistivity to be employed with arbitrary electrode arrangements. Laboratory trials of our extensions of electrical resistivity tomography to a complex form are reported. The inversion procedure is presented and demonstrated for a range of targets, with resistive and reactive characteristics. The approach is shown to provide useful magnitude and phase images, giving spectral information about the region of interest. Cole–Cole analysis of the inversion results reveals specific material relaxation characteristics. The usefulness of imaging complex resistivity is evident when compared with more conventional resistivity tomography, in particular when examined over a range of input frequencies. ©2000 Elsevier Science S.A. All rights reserved.

Keywords: Complex resistivity; Inversion; Relaxation

1. Introduction

Electrical conduction (charge transport) and polarisation (charge separation) belong to the fundamental physical properties of material media. The media of interest in geoscientific disciplines dealing with the earth's crust are basically minerals and rocks. A rock can be considered as a three-component system, consisting of grains, pores (which might be fluid-filled), and the corresponding interfaces. The electrical bulk properties of a rock depend on both the individual properties of these constituents and their geometrical arrangement within the rock.

Electrolytic conduction through the pore solution principally represents a purely resistive (i.e. in-phase) contribution to the bulk conductivity of a rock. However, interfacial conduction mechanisms, incident to electrical double layers at the grain surfaces, or abrupt changes in the conduction mode (e.g. from electrolytic to electronic in mineralised rocks) may give rise to induced polarisation effects and, thus, reactive (i.e. out-phase) conductivity components. The descriptive physical parameter of both conduction and polarisation phenomena at lower frequencies less than 10 kHz is the complex conductivity, or its reciprocal, complex resistivity. As a frequency-dependent complex number with both magnitude and phase, it fully describes the electrical response of

a rock to an electrical excitation and, thus, characterises its electrical behaviour.

Complex resistivity has been widely available for several decades in mineral prospecting industry. With this method impedance data (in terms of magnitude and phase) are collected over a range of input frequencies, typically in the mHz–kHz range, conventionally using electrodes on the ground surface. Applications of complex resistivity are by no means confined to mineral exploration. There is growing interest in using such information to gain an understanding about the hydraulic properties of the subsurface environment. Silts and loams, for example, may exhibit significant polarisation, which will be reflected in high phase shifts (see, for example, [10]). In comparison, coarse sands and gravels usually show small phase lags. The intergranular permeability of many rocks will be strongly correlated to pore space characteristics, which have been shown to affect the spectral response [2,11].

In addition to qualitative imaging of anomalous structures the Cole–Cole relaxation model has been used widely in mineral exploration (see, for example, [9]) to characterise properties of rocks in terms of their mineral composition. Since different grain size distributions and mineral types exhibit different types of relaxation spectra Cole–Cole analysis permits quantification of specific spectral properties which may be directly correlated with material type.

It is not just characteristics of the grains and pores within a porous medium that may exhibit characteristic spectra.

* Corresponding author.

Observations by [1,8,12] have shown how complex resistivity may give valuable information about contaminants in our groundwaters by examining relaxation behaviour for porous media contaminated with different hydrocarbons. Interest is now growing into using complex resistivity for contaminant identification.

We report here on controlled laboratory trials of our extensions of electrical resistivity tomography to a complex form. The inversion procedure is presented and demonstrated for three different targets, with resistive and reactive characteristics. The analysis is extended to recover intrinsic relaxation properties with a view to utilising the technique for target identification.

2. Forward problem

At a given measurement frequency $\omega = 2\pi f$ it is assumed that the region of interest may be represented as a two-dimensional complex resistivity distribution $\rho^*(x,z)$ (* denotes a complex term). If electromagnetic induction effects can be neglected the forward problem is defined by the Fourier transformed Poisson's equation for a point source with real current I :

$$\frac{\partial}{\partial x} \left(\frac{1}{\rho^*} \frac{\partial v^*}{\partial x} \right) + \frac{\partial}{\partial z} \left(\frac{1}{\rho^*} \frac{\partial v^*}{\partial z} \right) - \lambda^2 \frac{v^*}{\rho^*} = -I \delta(x) \delta(z). \quad (1)$$

In Eq. (1), v^* is the transformed complex potential and λ is the Fourier transformation variable. This differential equation may be solved using the finite element method for given boundary conditions. Inverse Fourier transform and appropriate superposition of the calculated potentials yields the complex transfer resistance of an arbitrary electrode configuration in the considered plane.

3. Inverse problem

The inversion procedure adopted here is based on the approach of [6] which is a development of the original 'Occam's inversion' developed by [4]. Within the inversion, log transformed parameters are used. The model vector \mathbf{m}^* and the data vector \mathbf{d}^* are defined as $m_j^* = \ln \rho_j^*$ ($j = 1, \dots, M$), $d_i^* = T_i^*$ ($i = 1, \dots, N$), where ρ_j^* are the complex resistivities of the individual cells of the finite-element mesh, T_i^* are the measured transfer impedances, M is the number of parameters, and N is the number of measurements.

The objective function being minimized in the inversion is composed of the complex L_2 measures of data misfit and first-order model roughness, with both terms being balanced by means of a regularization parameter α . Due to the nonlinearity of the problem, the minimization results in an iterative Gauss-Newton scheme, where at each step q the complex linear system of equations

$$\begin{aligned} & [A_q^{*H} W_d^{*H} W_d^* A_q^* + \alpha W_m^T W_m] \Delta \mathbf{m}_q^* \\ & = A_q^{*H} W_d^{*H} W_d^* [\mathbf{d}^* - \mathbf{f}^*(\mathbf{m}_q^*)] - \alpha W_m^T W_m \mathbf{m}_q^* \end{aligned} \quad (2)$$

is solved for a model update $\Delta \mathbf{m}_q^*$ by means of the conjugate-gradient method. In Eq. (2), \mathbf{m}_q^* is the current model, \mathbf{f}^* is the operator of the forward solution, A_q^* is the complex sensitivity matrix, W_d^* is a complex data weighting matrix, and W_m is the first-order model roughness matrix. H and T denote the Hermitian and transpose matrix, respectively. The data weighting matrix is given by $W_d^* = \text{diag}\{1/\varepsilon_1^*, \dots, 1/\varepsilon_N^*\}$, with (uncorrelated) complex data errors. Note that ε_i^* describes a confidence region ellipse in the complex plane around the data point d_i^* .

At each inverse iteration step a univariate search is performed to find the maximum value of α which locally minimizes the data misfit function or, respectively, yields the desired target misfit. The inverse iteration process is stopped when the desired data misfit target value is reached.

Within the forward modelling, all electromagnetic (EM) effects are assumed to be negligibly small. This consequently implies that either the considered frequency is sufficiently low or, at least, that any EM coupling is removed from the data prior to inversion. Here, the removal technique suggested by [5] is applied to the multifrequency data, in which the EM response at lower frequencies is described by means of an additive Cole-Cole dispersion term. For a Cole-Cole induced polarisation (IP) response, the individual transfer impedance spectra are fitted to the function

$$\begin{aligned} T^*(\omega) = T_0 \left\{ 1 - m_{ip} \left[1 - \frac{1}{1 + (i\omega\tau_{ip})^{c_{ip}}} \right] \right. \\ \left. \pm m_{em} \left[1 - \frac{1}{1 + (i\omega\tau_{em})^{c_{em}}} \right] \right\}, \end{aligned} \quad (3)$$

where T_0 is the dc (i.e. zero frequency) impedance, m_{ip} the chargeability, τ_{ip} the time constant, and c_{ip} the Cole-Cole exponent attributing to IP. Correspondingly, m_{em} , τ_{em} , and c_{em} describe the EM response. Finally, i denotes the imaginary unit. EM coupling is a complex function of wire layout and underlying resistivity distribution which may either cause an increase ('positive' EM coupling) or a decrease ('negative' EM coupling) of the observed phase lag in complex resistivity measurements. The variable sign in Eq. (3) accounts for both of these types. A Marquardt-type least-squares inversion is applied to find estimates of the two parameter sets, enabling the subsequent isolation of the IP response. The decoupled data sets then act as input to the inversion procedure outlined above.

4. Application to a scale model

4.1. Experimental setup

To demonstrate the approach a scale model was designed as follows (see also [13]). Two lines of 10 equally spaced

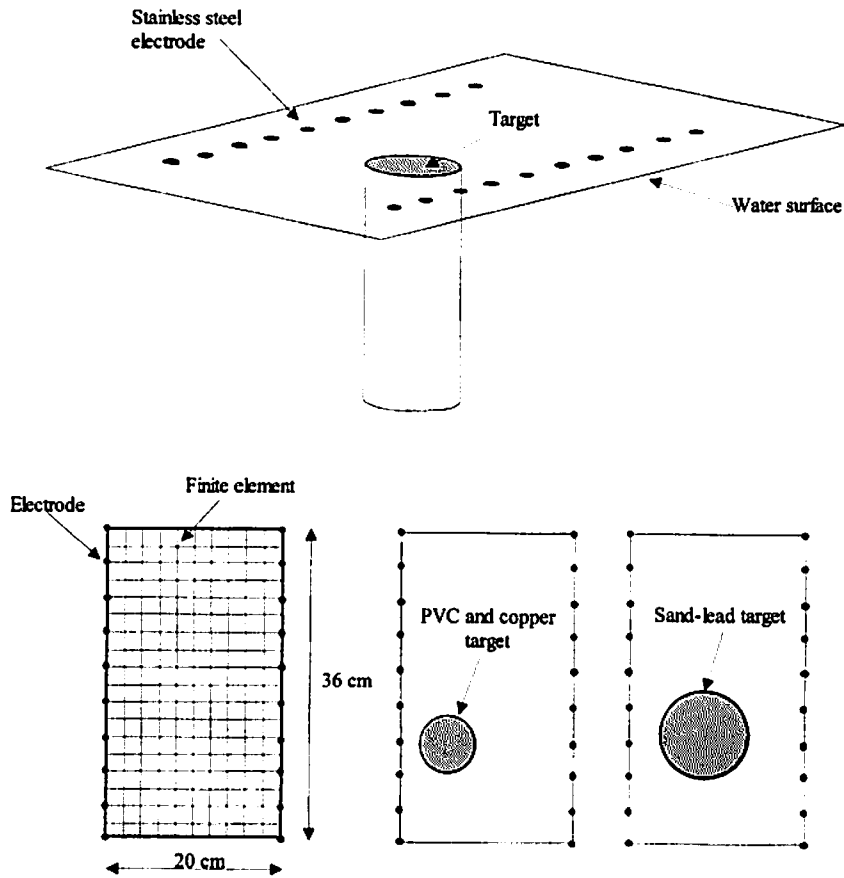


Fig. 1. Experimental layout and modelled region.

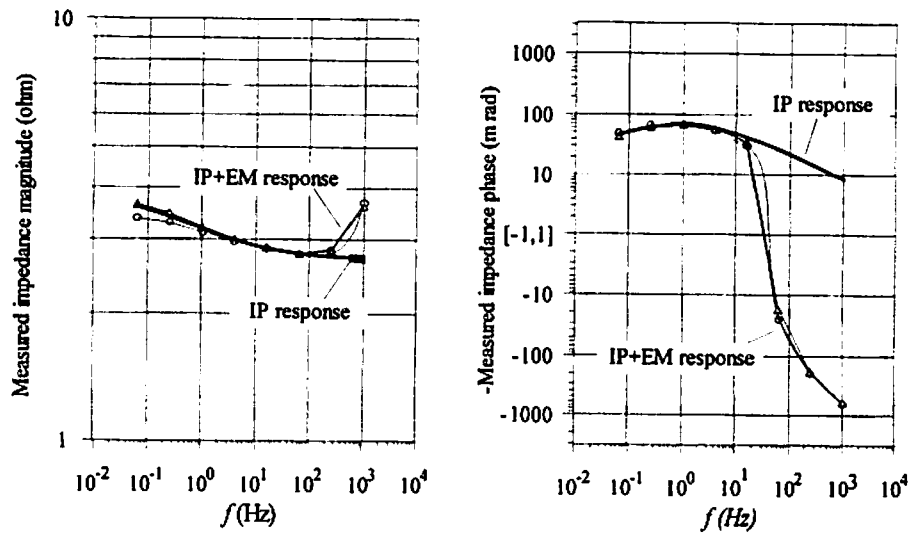


Fig. 2. Example of removal of electromagnetic coupling effects. Circle indicates 'normal' measurement and triangle indicates 'reciprocal' measurement. The curve through these points shows fitted double (IP + EM) Cole-Cole model response. The thick solid line shows the IP response alone.

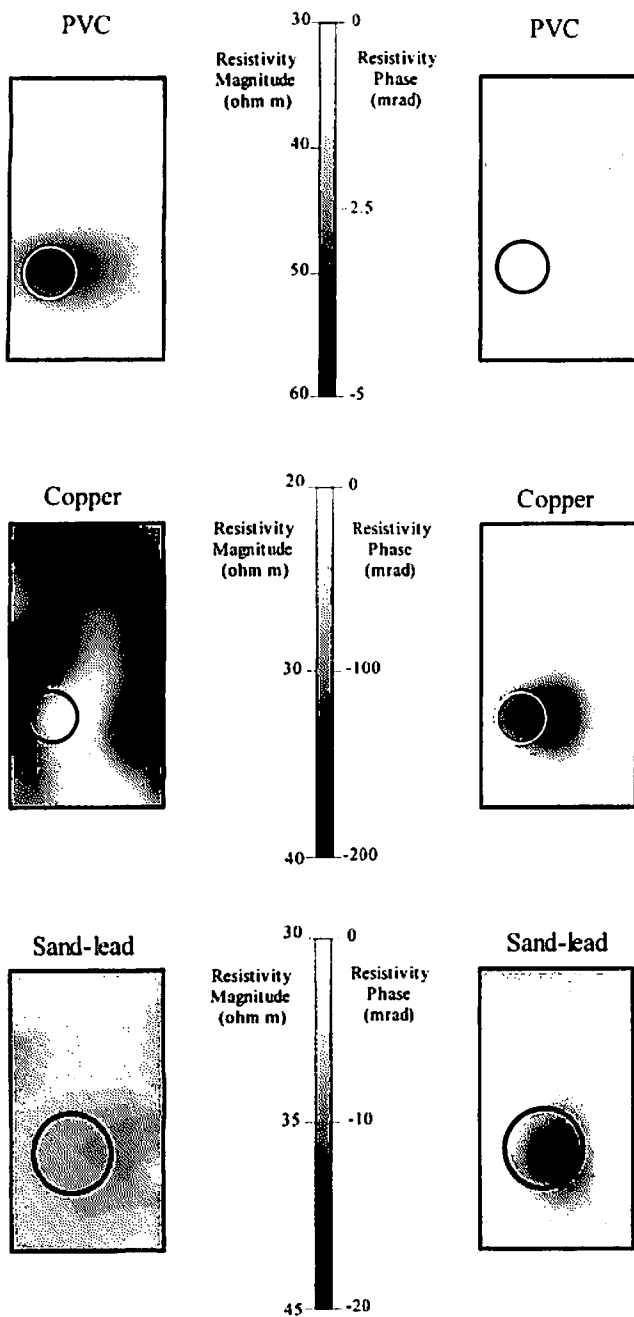


Fig. 3. Example results of the complex resistivity inversion at $f=4$ Hz.

stainless steel electrodes were aligned in parallel, 20 cm apart. The electrodes, each of which 2 mm diameter and 2 mm thick, were secured to a plastic frame and placed on the water surface in a 3.1 m diameter, 2.45 m deep fibreglass water tank filled with saline water. This arrangement was adopted as a scale model of a typical cross borehole electrode arrangement (the water tank acting as a 'half infinite' domain). The resistivity of the water within the tank was equivalent to a uniform 32Ω m.

Three targets were prepared: (1) a resistive target — a PVC tube, 6.7 cm in diameter; (2) a metallic target — the PVC tube with copper tape secured along the length of the

tube; and (3) an intermediate target — a cloth bag containing a mixture of sand and lead shot (2 parts sand and 1 part by volume of no. 7.5 lead shot), approximately 11 cm in diameter and 17 cm long. Each target was placed with its long axis perpendicular to the plane of the 'cross-borehole' arrangement of electrodes. Fig. 1 shows the arrangement, along with the finite-element parameterisation used within the inversion.

Complex resistance data were collected for all the target types. Each measurement is the impedance measured between two electrodes with current injected at two other electrodes. Each data set consists of 340 measurements, half of which were reciprocal measurements (current and potential electrodes switched) in order to assess error levels in the data. For each target, measurements were made at a number of current injection frequencies in order to assess any spectral characteristics and understand possible limitations in the field. Details of the data acquisition system can be found in [3].

Fig. 2 illustrates the EM effect on measured data, here specific measurements for the copper target are plotted in 'normal' and 'reciprocal' electrode arrangement together with the fitted Cole–Cole combined IP–EM response, as in Eq. (3), and the fitted response with EM effect removed. For frequencies above 64 Hz, EM effects can be seen to dominate the measurements and thus data collected above this frequency were not used for inversion.

4.2. Inversion results

Fig. 3 shows example results for the three targets. Results are shown for $f=4$ Hz frequency in terms of magnitude and phase produced by the inversion algorithm above. Also shown is the location of the target.

For the PVC target, as expected, the resistive anomaly is clearly shown in the magnitude image. The phase image reveals negligible reactive component in the data (typically less than 2 mrad). For the copper target the results demonstrate clearly that, for this particular target, the inversion is able to satisfactorily identify both a variation in real and imaginary components of the resistivity structure. Here the phase anomaly is two orders of magnitude greater than the PVC case. This serves as a useful demonstration of the algorithm under development. The sand–lead (acting as an intermediate target) reveals uniform resistive characteristics but is clearly identified by a significant phase response, albeit much smaller than the metallic target.

4.3. Spectral properties

Complex resistivity may provide additional information about the composition of the target of interest, however, the method, when used in a spectral manner, may also yield additional characteristics about the body under investigation.

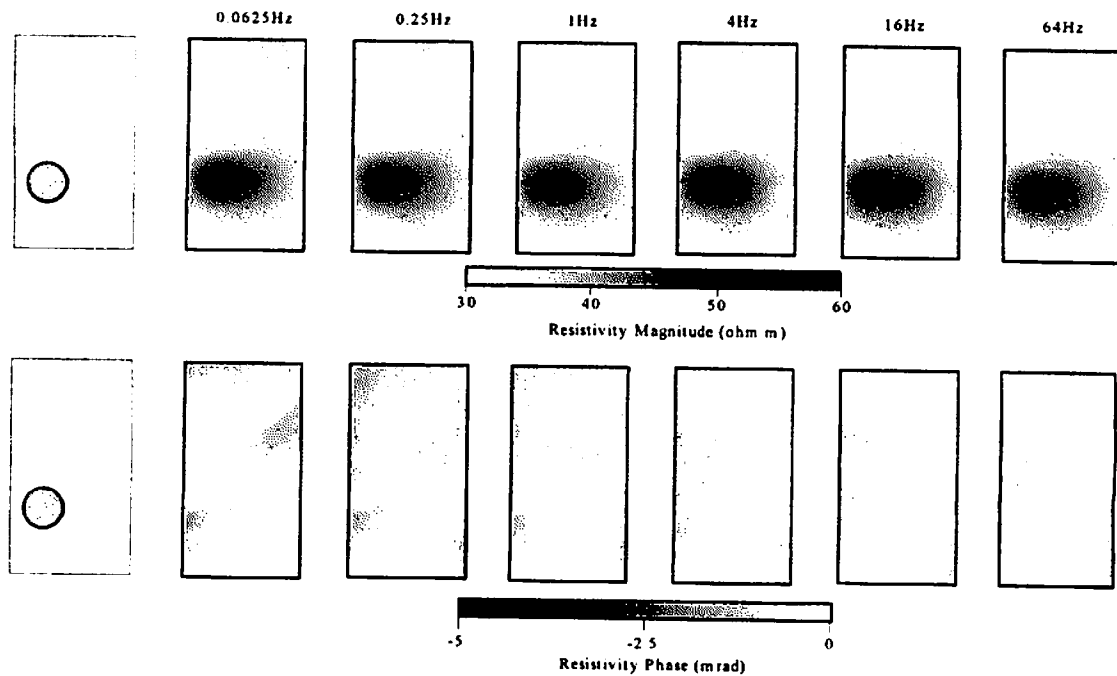


Fig. 4. Example results of the complex resistivity inversion using the 'PVC target'.

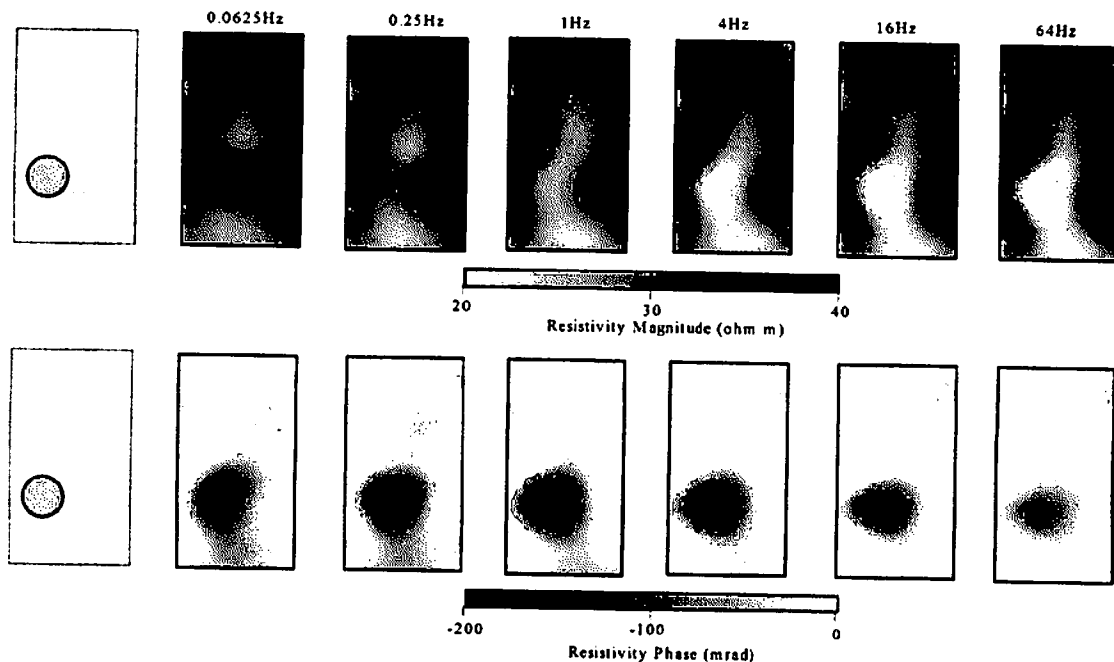


Fig. 5. Example results of the complex resistivity inversion using the 'copper target'.

Fig. 4 shows results of the complex inversion for the PVC target over a range of frequencies (0.0625–64 Hz).

The PVC target results reveal a clear resistive anomaly throughout all applied frequencies, with little variation in the magnitude. The phase images show very low, typically less than 2 mrad, values even at the highest frequencies. As the phase signals of the target here are so low (theoretically zero) the images act as a useful guide for the combined effect of measurement and modelling errors.

The copper target results in Fig. 5 show a contrasting result. Here the magnitude shows some change over applied frequency, more important perhaps is the phase response with frequency. Here the target signals appear to dominate any erroneous phase in the data and consequently the images show a clear phase feature at the location of the copper tube target, even at the 64 Hz frequency. Note that a peak phase response is seen at approximately 1 Hz which is consistent with measured response (see, for example, Fig. 2).

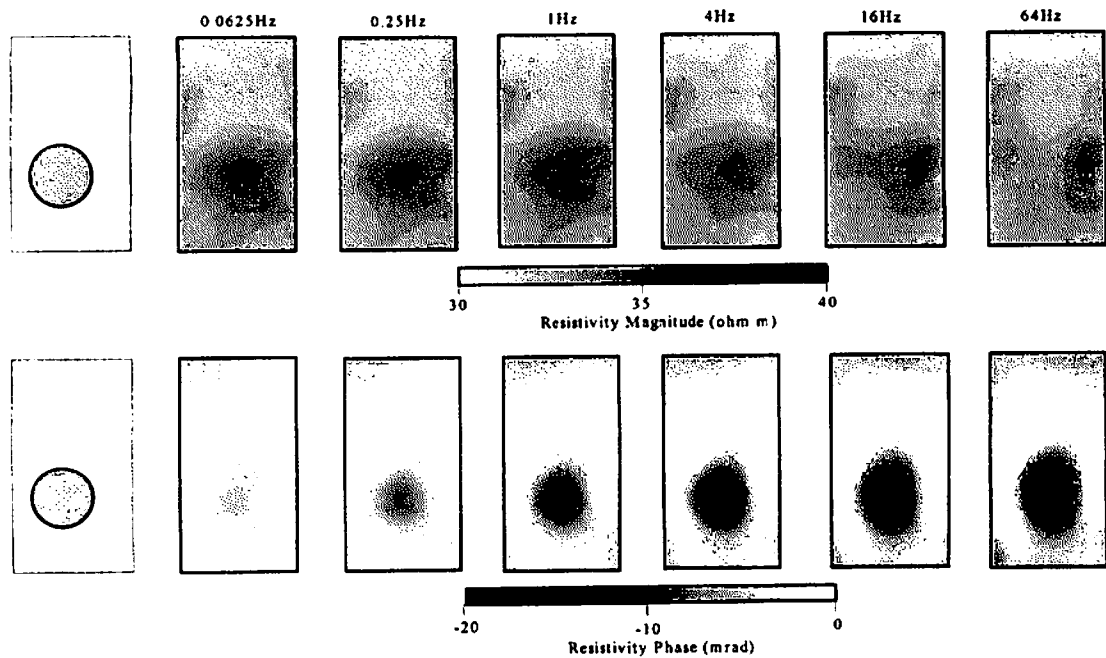


Fig. 6. Example results of the complex resistivity inversion using the 'sand-lead target'.

Fig. 6 illustrates the corresponding results for the sand-lead target. Here the resistive component can be seen in the magnitude images at low frequency whereas the phase images show a contrasting behaviour to the metallic target results, with gradual increase in reactive component over the frequencies shown.

To investigate further and quantify the change in complex resistivity with frequency it is necessary to examine individual parameter values. Representative parameters were selected for the copper and sand-lead target results for this purpose, Fig. 7 shows the location of the pixels used. Cole-Cole analysis of the pixel complex resistivities obtained directly from the inversion results are shown in Fig. 7. Here the IP response is described by fitting to the pixel values the curve

$$\rho^*(\omega) = \rho_0 \left\{ 1 - m_{ip} \left[1 - \frac{1}{1 + (i\omega\tau_{ip})^{c_{ip}}} \right] \right\}, \quad (4)$$

where ρ_0 is the dc resistivity. Note that in Eq. (4) the chargeability m_{ip} , the time constant τ_{ip} , and the Cole-Cole exponent c_{ip} now represent 'intrinsic' IP properties, in contrast to Eq. (3), where they just refer to the 'apparent' IP response as observed in the impedance spectrum.

The pixel spectra can be seen in Fig. 7 for the copper and sand-lead targets. The two objects clearly show different relaxation characteristics. Table 1 reports the Cole-Cole parameters for these specific curves. ρ_0 represents the zero-frequency asymptote of the target resistivities. Although of minor relevance in practical applications, it is a useful descriptive parameter by which the two targets are clearly discriminated.

The chargeability m_{ip} is a normalised measure of the IP amplitude, basically related to the amount of the material

giving rise to the effect (e.g. electronic conducting particles). Here, the recovered value for the continuously copper-coated PVC tube is significantly larger than that for the sand probe with only fractions of lead shot.

The characteristic time constants yield information on the spatial scales at which the polarisation phenomena take place. As expected, the value for the lead-sand target, involving smaller grains, is much smaller than that of the copper target. Empirically, a proportionality $\tau_{ip} \sim r^2$ has been found between the Cole-Cole time constant and the dominant grain size, r , for mineralised rocks (e.g. [7]). Adopting this relation for the copper tube and the lead shot with diameters of 6.7 cm and about 2 mm, respectively, would suggest a discrepancy between the corresponding IP relaxation times of approximately three orders of magnitude. This is in fair accordance with the results gained by complex resistivity tomography in Table 1.

The resultant frequency dependence c_{ip} for the copper target is close to 0.5, indicating that the copper-water interface behaves like a pure Warburg impedance as typical for polarisation phenomena dominated by diffusive processes (e.g. [7]). However, the somewhat smaller value for the sand-lead

Table 1
Cole-Cole parameters for copper and sand-lead targets (see Fig. 7 for pixel location in image)

Parameter	Target	
	Copper	Sand-lead
Dc resistivity ρ_0	52 Ω m	35 Ω m
Chargeability m_{ip}	0.77	0.15
Time constant τ_{ip}	1.45 s	3.2 ms
Exponent c_{ip}	0.42	0.36

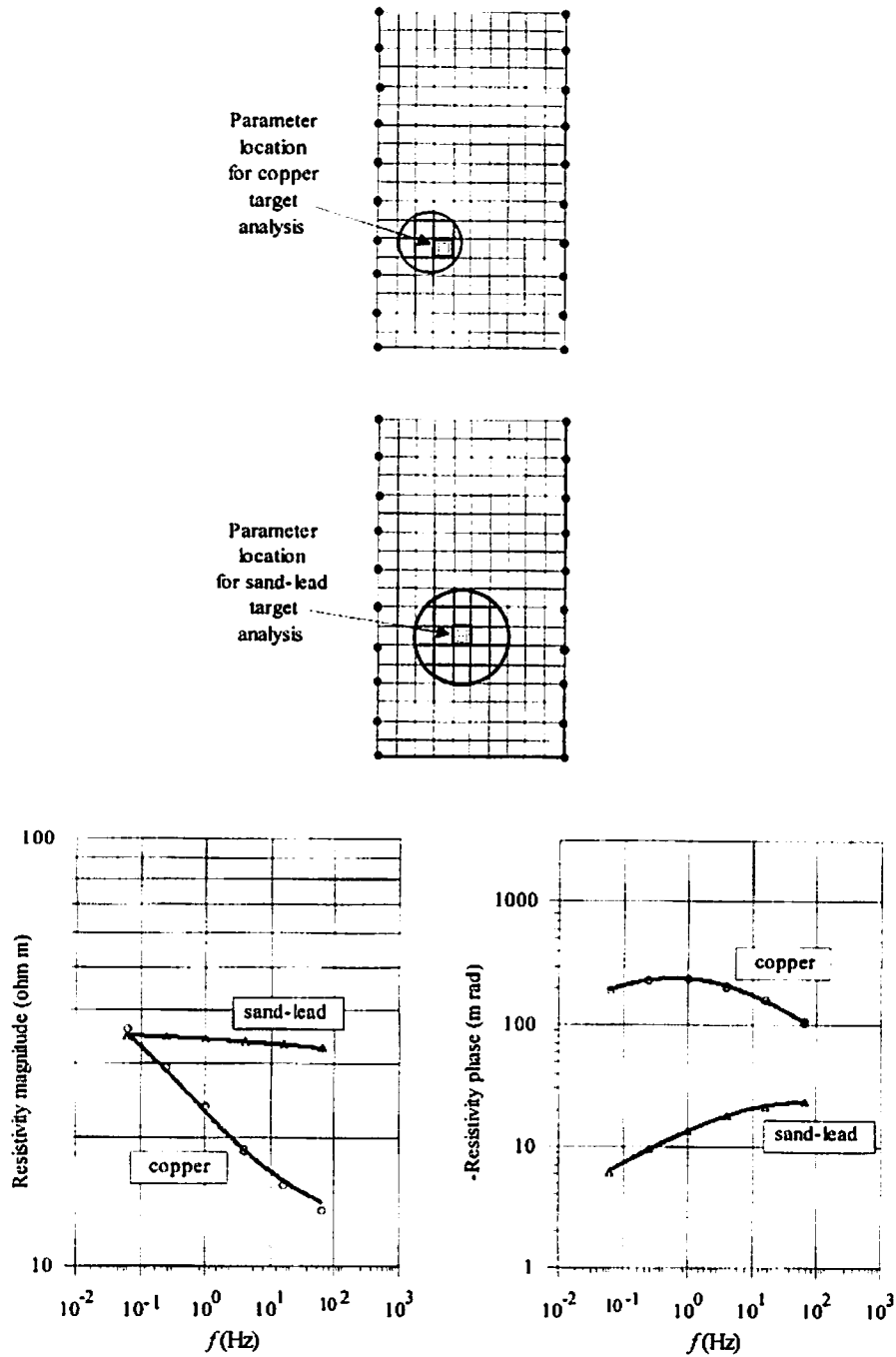


Fig. 7. Spectral properties of selected pixel values. Figure shows location of parameter value used from copper and sand-lead target inversions and fitted Cole–Cole curves.

mixture suggests that here other mechanisms, related to the porous character of the target, play a role as well in the formation of the spectral IP response.

5. Conclusions

With new tomographic inversion methods, such as those presented here, it is, in theory, possible to now apply complex resistivity imaging to arbitrary electrode arrangements.

These may be in a borehole to borehole arrangement or geometry more typical of biomedical or process tomography studies. Tomographic methods are likely to play a major role in these new investigations. With suitable techniques for removal of electromagnetic coupling effects data quality can be improved significantly so that small reactive components in the signal can be determined. What remains to be seen is the resolution and accuracy required in data acquisition in order to be able to satisfactorily distinguish material and pore fluid changes in the real subsurface environment.

The demonstration here has focussed on simple, exemplary targets with significantly different characteristics. Whereas to the PVC and the copper target a more illustrative character must be attributed in terms of the general complementary information provided by complex resistivity tomography, the sand–lead probe even represents a realistic target type encountered in possible geophysical applications related to mineral exploration. However, practical applications to environmental characterisation problems are likely to be limited to more subtle contrasts and, in addition, more complicated target geometries.

Data collection and analysis over a range of frequencies has been shown to give useful information about the nature of tomographic targets. Relaxation characteristics may be the link between electrical properties and the actual process of interest, for example fluid permeability, pore space characteristics, or mineral composition of rocks.

Acknowledgements

We are grateful for the constructive comments from Lee Slater and two anonymous referees.

References

- [1] F.D. Börner, M. Grühne, J.H. Schön, Contamination indications derived from electrical properties in the low frequency range, *Geophys. Prosp.* 41 (1993) 83–98.
- [2] F.D. Börner, J.R. Schopper, A. Weller, Evaluation of transport and storage properties in the soil and groundwater zone from induced polarization measurements, *Geophys. Prosp.* 44 (1996) 583–601.
- [3] W. Daily, A. Ramirez, K. Zonge, A unique data acquisition system for electrical resistance tomography. In: *Proc. Symp. Application of Geophysics to Engineering and Environmental Problems*, Environ. Eng. Geophys. Soc., 1996, pp. 743–751.
- [4] C. deGroot-Hedlin, S. Constable, Occam's inversion to generate smooth two-dimensional models from magnetotelluric data, *Geophysics* 55 (1990) 1613–1624.
- [5] P.G. Hallof, W.H. Pelton, The removal of inductive coupling effects from spectral IP data. In: *50th Annual Int. Meeting of the Soc. Expl. Geophys.*, Expanded Abstracts, 1980, pp. 2681–2724.
- [6] A. Kemna, A. Binley, Complex electrical resistivity tomography for contaminant plume delineation. In: *Proc. 2nd Meeting on Environmental and Engineering Geophysics*, Environ. Eng. Geophys. Soc., Eur. Section, 1996, pp. 196–199.
- [7] G.R. Olhoeft, Low-frequency electrical properties, *Geophysics* 50 (1985) 2492–2503.
- [8] G.R. Olhoeft, Direct detection of hydrocarbon and organic chemicals with ground-penetrating radar and complex resistivity. In: *Proc. NWWA/API Conf. on Petroleum Hydrocarbons and Organic Chemicals in Ground Water — Prevention, Detection, and Restoration*, 1986, pp. 284–305.
- [9] W.H. Pelton, S.H. Ward, P.G. Hallof, W.R. Sill, P.H. Nelson, Mineral discrimination and removal of inductive coupling with multifrequency IP, *Geophysics* 43 (1978) 588–609.
- [10] J.H. Schön, *Physical Properties of Rocks — Fundamentals and Principles of Petrophysics*, Handbook of Geophysical Exploration, Seismic Exploration 18, Elsevier, Amsterdam, 1996.
- [11] J.T. Sturrock, D.P. Lesmes, F.D. Morgan, The influence of micro-geometry on the hydraulic permeability and the induced polarization response of sandstones. In: *Proc. Symp. Application of Geophysics to Engineering and Environmental Problems*, Environ. Eng. Geophys. Soc., 1998, pp. 859–867.
- [12] H. Vanhala, Mapping oil-contaminated sand and till with the spectral induced polarization (SIP) method, *Geophys. Prosp.* 45 (1997) 303–326.
- [13] A. Ramirez, W. Daily, A. Binley, D. LaBrecque, Electrical impedance tomography of known targets, *J. Environ. Eng. Geophys.* 4 (1999) 11–26.